Japanese Journal of Applied Physics **56**, 127301 (2017)
https://doi.org/10.7567/JJAP.56.127301

REGULAR PAPER

Sound intensity probe for ultrasonic field in water using light-emitting diodes and piezoelectric elements

Xi Zeng*, Yosuke Mizuno, and Kentaro Nakamura

Laboratory for Future Interdisciplinary Research of Science and Technology, Tokyo Institute of Technology, Yokohama 226-8503, Japan

*E-mail: zeng.x.ab@m.titech.ac.jp

Received May 10, 2017; accepted September 6, 2017; published online November 9, 2017

The sound intensity vector provides useful information on the state of an ultrasonic field in water, since sound intensity is a vector quantity expressing the direction and magnitude of the sound field. In the previous studies on sound intensity measurement in water, conventional piezoelectric sensors and metal cables were used, and the transmission distance was limited. A new configuration of a sound intensity probe suitable for ultrasonic measurement in water is proposed and constructed for trial in this study. The probe consists of light-emitting diodes and piezoelectric elements, and the output signals are transmitted through fiber optic cables as intensity-modulated light. Sound intensity measurements of a 26 kHz ultrasonic field in water are demonstrated. The difference in the intensity vector state between the water tank with and without sound-absorbing material on its walls was successfully observed.

1. Introduction

It is essential to determine the sound pressure distribution in the ultrasonic field[1] both in industrial applications and fundamental researches[2,3] on high-intensity ultrasonic waves in liquid. Piezoelectric (PZT) hydrophones have long been used as a common tool to measure ultrasonic fields.[4,5] Optical techniques such as the Schlieren method[6–9] and the use of fiber optic hydrophones[10–15] are also used as alternatives. On the other hand, sound intensity measurement is a well-established method of determining the state of sound fields in the audible range in air, since sound intensity is a vector quantity expressing both the direction and the magnitude of the energy flow transmitted by sound waves.[16] A sound intensity probe consisting of multiple condenser microphones is commercially produced by several companies and widely used for noise source measurements. Moreover, sound intensity measurements have been applied to underwater sound fields.[17–19] Piezoelectric hydrophones were used instead of condenser microphones for underwater applications. However, the length of the metal cable is limited owing to the high output impedance of piezoelectric hydrophones. This sometimes causes practical difficulties in measuring ultrasonic fields in water since the electronics for instrumentation should be placed in a dry area and a long transmission distance is required. For industrial applications of high-power ultrasound, this usually becomes a problem since large water tanks are used in commercial factories and the transmission distance is rather long.

Multiple sensors are required for sound intensity measurement because the intensity is defined as the product of sound pressure and particle velocity. Particle velocity is usually calculated from the gradient of sound pressure, and a pair of pressure sensors are used to determine particle velocity. To find the two- or three-dimensional intensity vector, two or three pairs of pressure sensors are needed. As a result, the number of coaxial cables increases for practical sound intensity measurement. The problems of both the number and the length of metal cables are practical limitations in intensity measurement in water. These limitations make intensity measurement impossible in the case of huge tanks used in industrial applications.

The authors proposed a novel hydrophone configuration in which a light-emitting diode (LED) and a fiber optic cable are integrated with a piezoelectric element.[20–22] Sound pressure is transformed to electrical voltage through the piezoelectric effect, and transformed again to optical signal using the LED. The optical signal is transmitted through the fiber optic cable. Using this technology, intensity measurement in water will become more streamlined because there is little limitation in extending cable length and the weight of the cable can be reduced markedly.

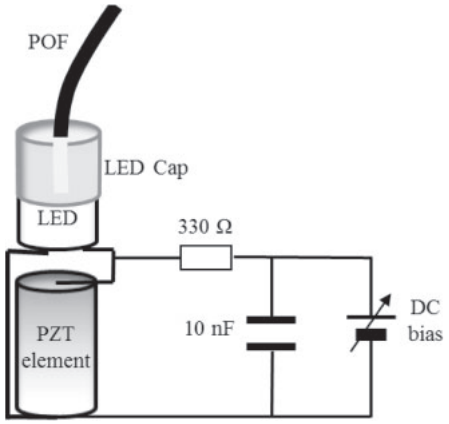

Fig. 1. Configuration of single LED-PZT sensor.

In this study, we integrate four of the ultrasonic sensors using LEDs and piezoelectric elements to a novel sound intensity probe for an ultrasonic field in liquid. To verify the operation of the proposed intensity probe, the measurement of the sound intensity distribution in a water bath is demonstrated for ultrasonic excitation at approximately 26 kHz. The difference between the measurements with and without sound-absorbing material on the walls of the bath was successfully observed from the intensity vector patterns measured using the proposed probe.

2. LED-PZT sound intensity probe

2.1 Basic structure of LED-PZT sensor

Figure 1 shows the configuration of the sound pressure sensor with LED and a piezoelectric element. An LED is directly connected to a cylindrical PZT element (5 mm in diameter and 10 mm in height). Here, the piezoelectric element

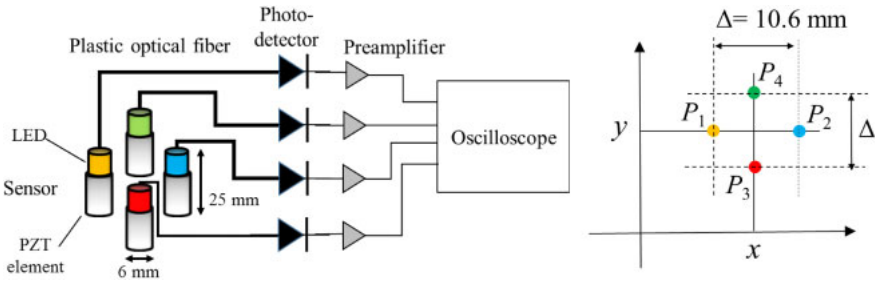

Fig. 2. (Color online) Configuration of four-channel LED-PZT intensity probe.

is made of lead zirconate titanate ceramics and polarized in its axial direction. Its top and bottom surfaces are electroplated with thin silver layers. The leads of the LED are soldered to the electrodes. A DC bias is provided via a 330 Ω resistor and a 10 nF capacitor. The operation voltage of the LED is set in the linear region beyond the threshold voltage by adjusting the DC power supply. When sound pressure at an ultrasonic frequency is applied to the PZT element, an AC voltage is induced across the PZT element, leading to the modulation of the LED current and thus the optical output. The dynamic change in the LED output is proportional to that in sound pressure. An optical signal is led to a detector located at a remote place using a plastic optical fiber (POF) with a diameter of 1 mm. A metal cap is attached to the LED to firmly connect the POF cable.

2.2 Sound intensity probe with LED-PZT sensors

Four LED-PZT sensors are integrated into a two-dimensional sound intensity probe, as illustrated in Fig. 2. The outputs of the sensors are received by four independent photodiodes with amplifiers through four POF cables. There is no need to use different colors for the light sources in this setup, however, four colors at wavelengths of 660 (red), 606 (amber), 520 (green), and 465 nm (blue) are selected for the LEDs. This is because, in future studies, wavelength division multiplexing (WDM) should be attempted over a single fiber cable to handle a larger number of sensors. In this paper, different wavelengths (colors) of light sources are employed for the preliminary investigation. The use of different colors provides a practical advantage in identifying the channel at the other end of fiber cables even in the case of using a four-channel sensor head.

Figure 3 shows the photodetector outputs versus the DC bias voltage of the four LED-PZT sensors. The bias DC voltages for the red, amber, green, and blue sensors are set at 2.8, 3.0, 3.5, and 3.8 V, respectively, so that all the DC optical outputs at the photoreceivers would fall at around the center of the dynamic range of the photodetector circuit. The sensors do not respond to low sound pressure without the bias voltage. The slopes of the linear part for the four LED-PZT sensors are nearly the same. However, the acoustic sensitivities are distributed by a factor of two, as measured and plotted in Fig. 4. Here, sound pressure was measured with a widely used hydrophone, Brüel&Kjær, 8103, with calibrated absolute sensitivity. The developed LED-PZT sensors showed good linearity up to 10 kPa. The differences among the outputs might be due to the difference in the waterproof coating of the PZT elements and the variation in the optical coupling between the LED and the fiber. The weight of one LED-PZT sensor, including a 6 m fiber cable,

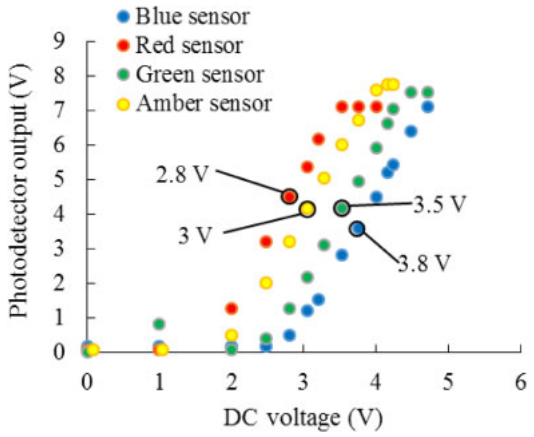

Fig. 3. (Color online) Output voltages of the photodetectors as functions of the DC voltage applied to the four LEDs. The operation points are indicated with black circles.

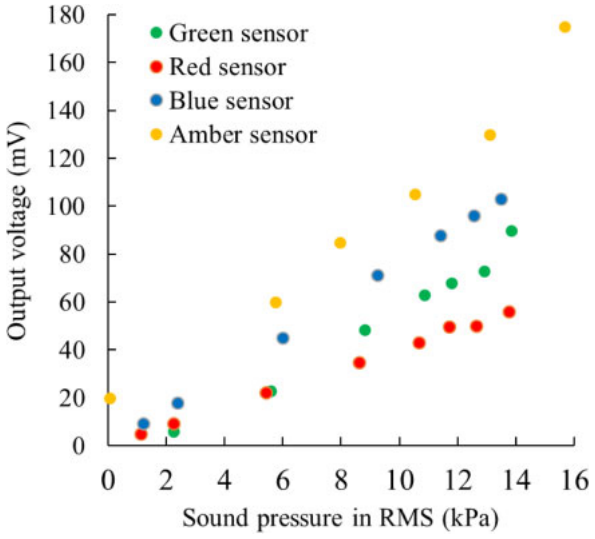

Fig. 4. (Color online) Output voltages of sensors as functions of applied sound pressure.

was 52 g, while that of the commercialized hydrophone (Brüel&Kjær 8103) with the same length of cable is 156 g. The weight of a conventional hydrophone is three time greater than a LED-PZT sensor.

3. Signal processing for sound intensity

3.1 Definition of sound intensity

Sound intensity, also known as acoustic intensity, is defined as the power flow across a unit area and measured in W/m^2.

The sound intensity $\boldsymbol{I}$ is a vector quantity and given by the product of the sound pressure p and the particle velocity vector $\boldsymbol{v}$ as

$$\boldsymbol{I} = p\boldsymbol{v}. \tag{1}$$

This expression gives instantaneous intensity, and the time-averaged value is usually used in practical sound intensity measurement since the time-averaged intensity gives the net energy flow, which is called "active intensity".

3.2 Complex expression of sound intensity

Assuming a sinusoidal continuous sound field, a complex expression is applied for sound pressure and particle velocity. The complex sound pressure $\tilde{P}$ and particle velocity vector $\tilde{V}$ are written using their amplitudes and phases P, V, φ, and θ as

$$\tilde{P} = Pe^{j\varphi}, \tag{2}$$

$$\tilde{V} = Ve^{j\theta}, \tag{3}$$

respectively, where j denotes the imaginary unit. Thus, the active intensity I is expressed as the real part:[23)]

$$I = \frac{1}{2}\mathrm{Re}[\tilde{P}\tilde{V}^*]. \tag{4}$$

Here, V^* is the complex conjugate of V. The imaginary part J, which is referred to as "reactive intensity", implies the stored energy in a standing wave field:

$$J = \frac{1}{2}\mathrm{Im}[\tilde{P}\tilde{V}^*]. \tag{5}$$

3.3 Sound intensity measurement with discrete points of sound pressures

Particle velocity is calculated from the finite difference in sound pressures at adjacent points, since only sound pressure is actually measurable with the sensor. From the equation of motion

$$j\omega\rho\tilde{V} = \mathrm{grad}\tilde{P}, \tag{6}$$

the particle velocity vector $\tilde{V} = (\tilde{V}_x, \tilde{V}_y)$ is written in finite difference forms as

$$\tilde{V}_x = \frac{\tilde{P}_2 - \tilde{P}_1}{j\omega\rho\Delta}, \tag{7}$$

$$\tilde{V}_y = \frac{\tilde{P}_4 - \tilde{P}_3}{j\omega\rho\Delta}. \tag{8}$$

Here, ω, ρ, and Δ are the angular frequency, the density of media, and the small distance between the two pressure measurement points. $\tilde{P}_1$, $\tilde{P}_2$, $\tilde{P}_3$, and $\tilde{P}_4$ are the complex sound pressures measured at the positions shown in Fig. 2. The amplitudes and phases for these sound pressures are P_1, P_2, P_3, P_4, φ_1, φ_2, φ_3, and φ_4, and their values will be actually measured in the experiments, as stated in Sect. 4.

$$\tilde{P}_i = P_i e^{j\varphi_i} \quad (i = 1, 2, 3, 4) \tag{9}$$

Using these measured values, the active components of the sound intensities I_x and I_y are written as

$$I_x = \frac{1}{2}\mathrm{Re}[\tilde{P}\tilde{V}_x^*] = \frac{P_1P_2}{2\omega\rho\Delta}\sin(\varphi_2 - \varphi_1), \tag{10}$$

$$I_y = \frac{1}{2}\mathrm{Re}[\tilde{P}\tilde{V}_y^*] = \frac{P_3P_4}{2\omega\rho\Delta}\sin(\varphi_4 - \varphi_3). \tag{11}$$

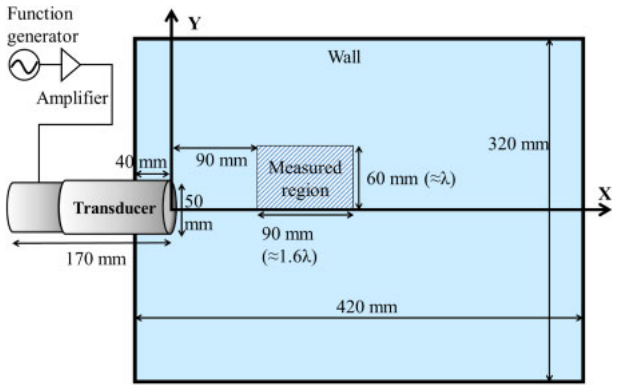

Fig. 5. (Color online) Measurement setup and coordinate system.

The reactive components J_x and J_y are written as

$$J_x = \frac{1}{2}\mathrm{Im}[\tilde{P}\tilde{V}_x^*] = \frac{P_2^2 - P_1^2}{4\omega\rho\Delta}, \tag{12}$$

$$J_y = \frac{1}{2}\mathrm{Im}[\tilde{P}\tilde{V}_y^*] = \frac{P_4^2 - P_3^2}{4\omega\rho\Delta}. \tag{13}$$

4. Measurement

4.1 Measurement setup

Figure 5 shows the setup and coordinate system for the demonstration of measurement. An ultrasonic transducer operating at 26.35 kHz is mounted on one of the walls of a water bath of $420 \times 320\,\mathrm{mm}^2$. The transducer is composed of a half-wavelength straight horn and a bolt-clamped Langevin transducer.[24)] The horn is clamped at its node to the wall and has a circular radiation surface of 50 mm diameter. The center of the transducer is 65 mm below the water surface and 110 mm above the bottom.

The LED-PZT sensor array scanned 117 positions in 7.5 mm steps in the two-dimensional region indicated in Fig. 5. This means 13 points along the X-axis and 9 points along the Y-axis. The x-component of sound intensity was always measured with the amber LED sensor (P_1) and the blue LED sensor (P_2), while the y-component was measured with the red LED sensor (P_3) and the green LED sensor (P_4). The spacing between sensors Δ was chosen to be 10.6 mm (Fig. 2), which corresponds to 0.186 times the wavelength of 26.35 kHz ultrasonic waves in water. The spacing Δ should be sufficiently smaller than the wavelength. However, it is known that a too small spacing amplifies noise in the finite difference calculation.[25)]

4.2 Reference result with piezoelectric hydrophone

Before sound intensity measurement with the proposed probe, the sound pressure distribution was measured using a conventional piezoelectric hydrophone (Brüel&Kjær 8103). The single hydrophone was mechanically scanned, and the amplitude is mapped in Fig. 6(a). A standing wave distribution is clearly observed along the x-direction. The measurement was conducted under almost the same conditions using the proposed four-channel LED-PZT sensor array. The average of four sensors is plotted in Fig. 6(b) on a linear scale. We carefully measured such that the center of the hydrophone and the LED-PZT sensor array were at the same depth in water. As can be seen from Figs. 6(a) and 6(b), standing wave patterns are observed. The error between these two results are possibly attributed to the instability of the

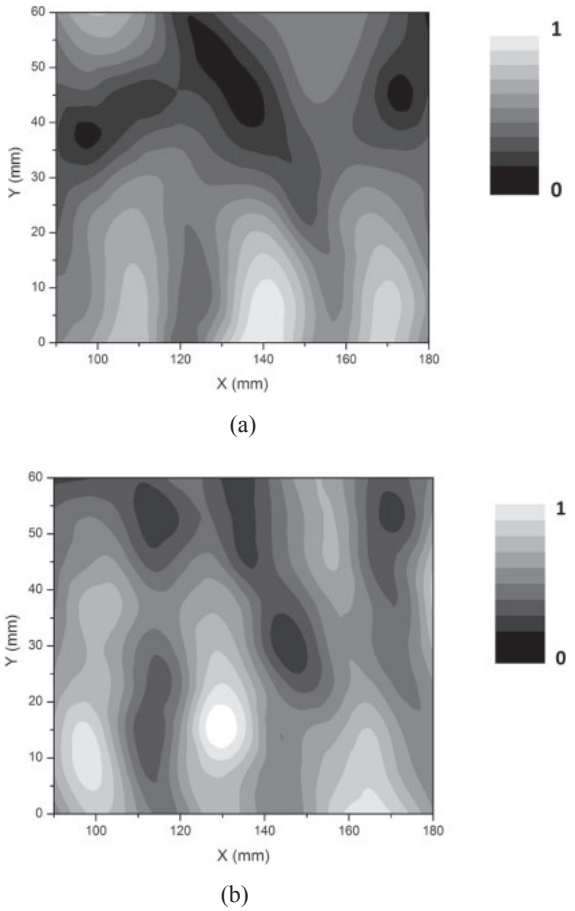

Fig. 6. Sound pressure distributions measured using (a) commercial piezoelectric hydrophone and (b) LED-PZT sensor array.

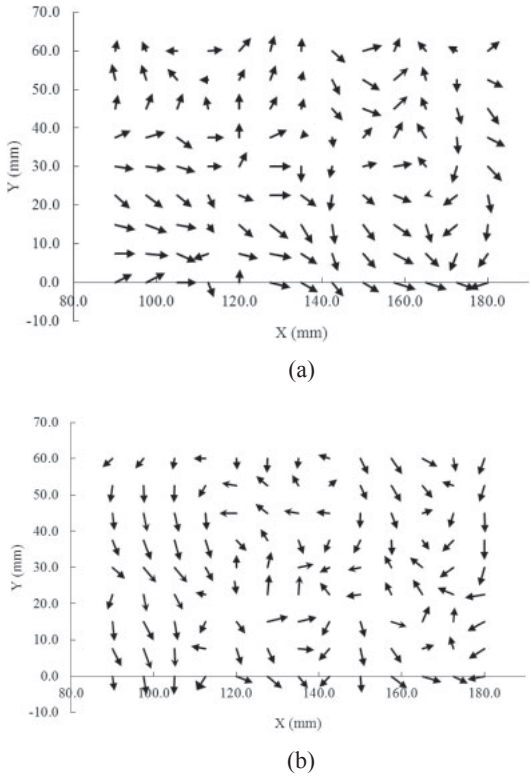

Fig. 7. Sound intensity distributions without sound-absorbing material in the water tank: (a) active intensity and (b) reactive intensity. The lengths of arrows are indicated on a logarithmic scale.

ultrasonic standing wave field, which was sensitive to the insertion of the sensors and water surface disturbance.

4.3 Sound intensity measurement

The active and reactive components of sound intensity vectors measured with the proposed LED-PZT array probe are shown in Figs. 7(a) and 7(b), respectively. Note that a logarithmic scale is adopted for determining the lengths of arrows. As no sound-absorbing material is set on the walls and a high reflection is expected at the walls, as well as at the water surface and the bottom, it is thought that a high standing wave field is excited.

As for the reactive intensity component, the direction of the x-components of arrows changed its periodicity from positive to negative along the x-axis. This is a typical nature of a standing wave field. The x-components of active intensity around the transducer axis are almost positive. However, little clear tendency is found in other places.

Next, sound-absorbing materials were fixed on all the walls and the bottom surfaces of the tank, except the water surface. We arranged the orientations of the sound-absorbing materials such that there exists no parallel pair of surfaces to suppress the generation of standing waves. Sponge with a corrugated surfaces was used as the sound-absorbing material. The depth of the corrugated surface was about 35 mm, which was 63% of the ultrasonic wavelength. We can expect a reduction in the standing waves generated to some extent by using this sound-absorbing material, but it should be noted that it is difficult in practice to fully suppress the reflections.

The results of measurement with sound-absorbing materials are shown in Fig. 8. The x-components in the active intensity vector are all positive over the measured region. As a whole, a positive overall flow is apparently observed in this result. As for the reactive intensity components, the x-components still alternated regularly from positive to negative along the x-axis. From these results, we can understand that the reflection was reduced when using the sound-absorbing material and the intensity of the traveling wave component increased. To compare the results in Fig. 7 and Fig. 8 more quantitatively, the average active intensity was calculated and its ratio to the reactive intensity is summarized in Table I. The intensity of the travelling wave component increased obviously in the case of the measurement with sound-absorbing material. Data shown in Figs. 7 and 8 are raw data without correction for the sensitivity of each LED-PZT sensor. In future research, we should develop a calibration procedure for the intensity probe.

In this experimental setup at this frequency, it was, in practice, very difficult to suppress the reflections from the walls, bottom, and water surface. As a result, we were unable to conduct the calibration under a pure traveling wave field. In addition, the three-dimensional structure of the acoustic field in the water bath might affect the results obtained using the two-dimensional probe developed here.

5. Conclusions

A two-dimensional sound intensity probe consisting of four channels of LED-PZT sensors was fabricated, and sound intensity measurement under water was conducted in the ultrasonic frequency range. The outputs of the sensors were

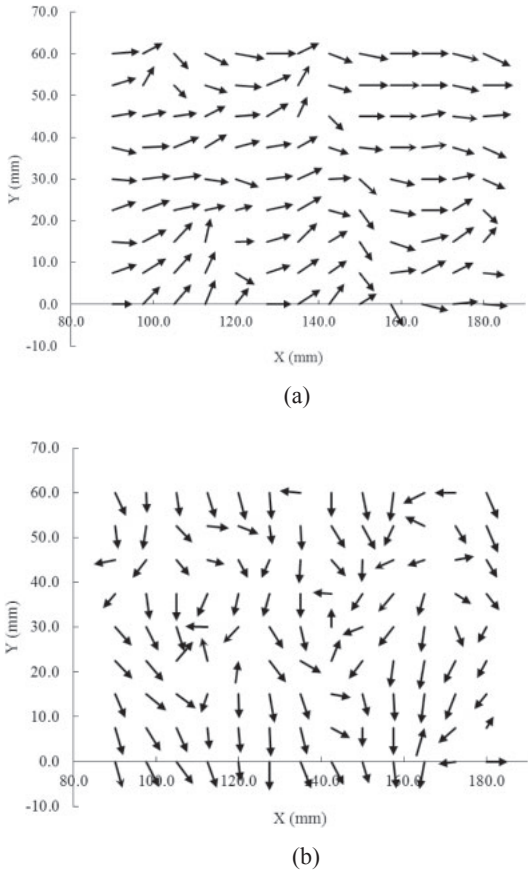

Fig. 8. Intensity distributions with sound absorbing material: (a) active intensity and (b) reactive intensity. The lengths of arrows are indicated in the logarithmic scale.

Table I. Ratio of active intensity to reactive intensity in the measured field.

	Average of top three positions	Average of all positions
Without sound-absorbing material in tank	0.9	1.0
With sound-absorbing material in tank	2.1	1.8

transmitted using plastic optical fibers and detected with four independent photodiodes. Intensity vector maps were drawn for both the high standing wave field and weakened reflection field at approximately 26 kHz. The results demonstrated the effectiveness of sound intensity measurements in the ultrasonic field in water. The use of optical fibers enabled easy handling of the cables between the sensor head and the electronics for signal processing. In this paper, we adopted four different colors of the LEDs and four separate fiber cables. We are expecting the possibility of transmitting optical signals over one fiber cable using the wavelength division multiplexing method.

In the future, first, we must establish a precise calibration method for the measurement system to obtain more precise results. Second, for three-dimensional measurements, the number of channels of the probe will be increased with the minimum number of optical fibers by adopting the wavelength division multiplexing method. The sensor elements shall be miniaturized using tip LEDs and smaller piezoelectric elements for higher frequency operation since high-power ultrasonic applications in the MHz range are extending in both industrial and medical fields.

1) K. Mizutani, N. Wakatsuki, and T. Ebihara, Jpn. J. Appl. Phys. **55**, 07KA02 (2016).
2) Y. Mochizuki, H. Taki, and H. Kanai, Jpn. J. Appl. Phys. **55**, 07KF13 (2016).
3) M. Omura, K. Yoshida, M. Kohta, T. Kubo, T. Ishiguro, K. Kobayashi, N. Hozumi, and T. Yamaguchi, Jpn. J. Appl. Phys. **55**, 07KF14 (2016).
4) P. A. Lewin, Ultrasonics **19**, 213 (1981).
5) M. Platte, Ultrasonics **23**, 113 (1985).
6) K. Yamomoto, in *Ultrasonic Transducers: Materials and Design for Sensors, Actuators and Medical Applications*, ed. K. Nakamura (Woodhead Publishing, Cambridge, U.K., 2012) p. 314.
7) T. Neumann and H. Ermert, Ultrasonics **44**, e1561 (2006).
8) M. Ohno, Jpn. J. Appl. Phys. **48**, 07GC10 (2009).
9) S. Oyama, J. Yasuda, H. Hanayama, S. Yoshizawa, and S. I. Umemura, Jpn. J. Appl. Phys. **55**, 07KB09 (2016).
10) W. B. Spillman, Jr. and D. H. McMahon, Appl. Phys. Lett. **37**, 145 (1980).
11) W. B. Spillman, Appl. Opt. **20**, 465 (1981).
12) J. Staudenraus and W. Eisenmenger, Ultrasonics **31**, 267 (1993).
13) Y. Zhou, L. Zhai, R. Simmons, and P. Zhong, J. Acoust. Soc. Am. **120**, 676 (2006).
14) C. Koch, Ultrasonics **34**, 687 (1996).
15) P. C. Beard and T. N. Mills, Electron. Lett. **33**, 801 (1997).
16) F. Jacobsen, in *Springer Handbook of Acoustics*, ed. T. D. Rossing (Springer, New York, 2015) p. 1093.
17) D. L. Hutt, P. C. Hines, and A. A. J. Hamilton, presented at OCEANS '99 MTS/IEEE, 1999.
18) K. J. Bastyr, G. C. Lauchle, and J. A. McConnell, J. Acoust. Soc. Am. **106**, 3178 (1999).
19) I. Gloza, Acta Phys. Pol. A **118**, 58 (2010).
20) K. Nakamura and T. Sugimoto, Denghi Joho Tsushin Gakkai Ronbunshi C **J-86C**, 1331 (2003) [in Japanese].
21) K. Nakamura and T. Sugimoto, presented at IEEE Ultrasonics Symp., 2007.
22) K. Nakamura, H. Ogura, and T. Sugimoto, Acoust. Imaging **29**, 309 (2008).
23) M. J. Crocker and J. P. Arenas, Acoust. Phys. **49**, 163 (2003).
24) H. Ito, H. Jimbo, K. Shiotani, and N. Sakai, Jpn. J. Appl. Phys. **55**, 07KC04 (2016).
25) L. Lapidus and G. F. Pinder, *Numerical Solution of Partial Differential Equations in Science and Engineering* (Wiley, New York, 1999) Chap. 1.